The Astrophysical Journal, 866:25 (5pp), 2018 October 10 https://doi.org/10.3847/1538-4357/aaddfb
© 2018. The American Astronomical Society. All rights reserved.

MMS Observations of Beta-dependent Constraints on Ion Temperature Anisotropy in Earth's Magnetosheath

Bennett A. Maruca[1], A. Chasapis[1], S. P. Gary[2], R. Bandyopadhyay[1], R. Chhiber[1], T. N. Parashar[1], W. H. Matthaeus[1,3], M. A. Shay[1,3], J. L. Burch[4], T. E. Moore[5], C. J. Pollock[6], B. J. Giles[5], W. R. Paterson[5], J. Dorelli[5], D. J. Gershman[5], R. B. Torbert[7], C. T. Russell[8], and R. J. Strangeway[8]
[1] Department of Physics & Astronomy, University of Delaware, Newark, DE, USA; bmaruca@udel.edu
[2] Space Science Institute, Boulder, CO, USA
[3] Bartol Research Institute, Newark, DE, USA
[4] Southwest Research Institute, San Antonio, TX, USA
[5] NASA Goddard Space Flight Center, Greenbelt, MD, USA
[6] Denali Scientific, Fairbanks, Alaska, USA
[7] University of New Hampshire, Durham, NH, USA
[8] University of California, Los Angeles, CA, USA
Received 2018 June 22; revised 2018 August 27; accepted 2018 August 28; published 2018 October 5

Abstract

Protons (ionized hydrogen) in the solar wind frequently exhibit distinct temperatures ($T_{\perp p}$ and $T_{\parallel p}$) perpendicular and parallel to the plasma's background magnetic field. Numerous prior studies of the interplanetary solar wind have shown that, as proton beta ($\beta_{\parallel p}$) increases, a narrower range of proton temperature anisotropy ($R_p \equiv T_{\perp p}/T_{\parallel p}$) values is observed. Conventionally, this effect has been ascribed to the actions of kinetic microinstabilities. This study is the first to use data from the *Magnetospheric Multiscale Mission* to explore such $\beta_{\parallel p}$-dependent limits on R_p in Earth's magnetosheath. The distribution of these data across the ($\beta_{\parallel p}$, R_p)-plane reveals limits on both $R_p > 1$ and $R_p < 1$. Linear Vlasov theory is used to compute contours of constant growth rate for the ion–cyclotron, mirror, parallel-firehose, and oblique-firehose instabilities. These instability thresholds closely align with the contours of the data distribution, which is consistent with these instabilities acting to limit extremes of proton temperature anisotropy in the magnetosheath.

Key words: instabilities – plasmas – solar wind – turbulence

1. Introduction

The solar wind consists of the highly ionized, strongly magnetized plasma that flows supersonically from the Sun's corona out into deep space. As the plasma approaches Earth, it crosses a bow shock, which reduces it to subsonic speeds and typically causes significant increases in the plasma's density and temperature. This region of subsonic solar-wind plasma between the bow shock and the Earth's magnetosphere is known as the magnetosheath.

The vast majority of ions in solar-wind plasma are protons, but α-particles still typically comprise at least a few percent. Because of the plasma's high temperature and low density, rates of Coulomb collisions remain low, and ions often deviate from thermal equilibrium. For example, different ion species frequently exhibit distinct temperatures and bulk velocities. Furthermore, because of the solar wind's strong magnetic-field, $\boldsymbol{B}$, the transport of energy in this plasma is direction dependent, which gives rise to temperature anisotropy. For protons, this effect is quantified by the ratio

$$R_p \equiv \frac{T_{\perp p}}{T_{\parallel p}} \tag{1}$$

where $T_{\perp p}$ and $T_{\parallel p}$ are respectively the proton temperatures perpendicular and parallel to $\boldsymbol{B}$. A value of $R_p = 1$ corresponds to temperature isotropy, which is a property of the equilibrium state.

As detailed below in Section 2, numerous studies have shown that the distribution of R_p-values observed in the solar wind depends strongly on the parameter

$$\beta_{\parallel p} \equiv \frac{n_p\, k_B\, T_{\parallel p}}{B^2/(2\,\mu_0)} \tag{2}$$

where n_p is the proton density, k_B the Boltzmann constant, and μ_0 the vacuum permeability. Essentially, $\beta_{\parallel p}$ is the ratio of the parallel proton pressure to the magnetic pressure. These studies have revealed that, for progressively larger $\beta_{\parallel p}$-values, the range of R_p-values observed in the solar wind narrows.

This study is the first to use data from the *Magnetospheric Multiscale Mission* (*MMS*) to study how R_p varies with $\beta_{\parallel p}$ in Earth's magnetosheath and to explore what role instabilities play in the process. Section 2 details prior observations of correlation of R_p with $\beta_{\parallel p}$ and overviews the theory of kinetic microinstabilities. Sections 3 and 4 respectively describe the specific *MMS* observations used in this study and how they were analyzed. A discussion of the results of this analysis is presented in Section 5.

2. Background

Numerous prior studies (see below) have shown that the values of proton temperature anisotropy, R_p, observed in the solar wind depend on the value of $\beta_{\parallel p}$. Specifically, the range of observed R_p-values narrows as the value of $\beta_{\parallel p}$ increases. This effect has been ascribed to the actions of kinetic microinstabilities, which are widely understood to impose constraints on temperature anisotropy in weakly collisional space plasmas via wave–particle scattering. Such constraints on protons have been demonstrated through hybrid simulations

(Gary et al. 1997) and (as described below) through observations of protons in the interplanetary solar wind (Hellinger et al. 2006), terrestrial magnetosheath (Gary et al. 1997), and terrestrial magnetosphere (Gary et al. 1995).

This section provides a brief overview of anisotropy-driven instabilities and their role in the evolution of the solar wind. The textbooks by Gary (1993) and Treumann & Baumjohann (1997) as well as the review articles by Schwartz (1980) and Yoon (2017) provide a far more detailed treatment of the subject. Likewise, Klein & Howes (2015) include a detailed treatment of the specific microinstabilities associated with proton temperature anisotropy.

A kinetic microinstability is an instability associated with the velocity distribution function (VDF) of one or more particle species in the plasma. Any deviation of a VDF from the entropically preferred Maxwellian VDF represents a potential source of free energy. If such a deviation becomes sufficiently large, a fluctuation may develop into a growing mode: its amplitude may increase exponentially until particles are scattered in phase space and the plasma is driven to a state closer to thermal equilibrium. In this way the thresholds of microinstabilities can act as limits on the plasma's deviation from equilibrium.

Proton temperature anisotropy may drive various instabilities if the value of $R_{\rm p} \equiv T_{\perp {\rm p}}/T_{\parallel {\rm p}}$ deviates sufficiently from unity. When $T_{\perp {\rm p}} > T_{\parallel {\rm p}}$, the ion–cyclotron instability and/or mirror instability may develop. Both arise from electromagnetic fluctuations but, for the former, these modes propagate parallel to the background magnetic field, $\boldsymbol{B}$, and, for the latter, the wave vectors have an oblique orientation to $\boldsymbol{B}$ and are non-propagating (i.e., have a phase speed of zero). The case of $T_{\parallel {\rm p}} > T_{\perp {\rm p}}$ may drive the parallel and/or oblique firehose instabilities which, as their names imply, arise from electromagnetic modes whose wave vectors are respectively oriented parallel or obliquely to $\boldsymbol{B}$.

Various studies (e.g., Gary 1993; Hellinger et al. 2006; Maruca et al. 2012; Klein & Howes 2015) based on linear Vlasov theory have predicted that the threshold $R_{\rm p}$-value for each of these four instabilities depends strongly on $\beta_{\parallel {\rm p}}$ and approaches $R_{\rm p} = 1$ at large $\beta_{\parallel {\rm p}}$-values. Consequently, a common method for searching for the effects of these instabilities in a plasma involves plotting the distribution of a large sample of observations over the ($\beta_{\parallel {\rm p}}$, $R_{\rm p}$)-plane.[9] The alignment of the data distribution with contours of constant growth rate, γ, for a given instability are conventionally interpreted as strong evidence for the action of that instability on the observed plasma.

The ($\beta_{\parallel {\rm p}}$, $R_{\rm p}$)-plane has been used extensively to study the impact of anisotropy-driven instabilities on protons in the interplanetary solar wind. Gary et al. (2001) and Kasper et al. (2002) were among the first to apply this type of analysis to a large sample of solar-wind measurements. Later, the seminal work of Hellinger et al. (2006) revealed that the oblique (i.e., mirror and oblique-firehose) instabilities are more active in limiting $R_{\rm p}$-values than the parallel (i.e., ion–cyclotron and parallel-firehose) instabilities—even for $\beta_{\parallel {\rm p}}$-values for which linear Vlasov theory predicts that the latter provide a stricter constraint on $R_{\rm p}$ than the former. Subsequent studies supported this conclusion and further developed the idea that instabilities may play an important role in how solar-wind plasma expands, develops fluctuations, and is heated (Matteini et al. 2007; Bale et al. 2009; Maruca et al. 2011; Wicks et al. 2013; Hellinger & Trávníček 2014; Verscharen et al. 2016). Likewise, the work of Osman et al. (2012, 2013) and Servidio et al. (2014) demonstrated enhancements in quantitative measures of turbulence in marginally unstable solar-wind plasma. Recently, some studies have begun refining the analysis of proton temperature anisotropy instabilities by incorporating the effects of proton beams (Klein et al. 2018) and of α-particle temperature anisotropy (Maruca et al. 2012; Bourouaine et al. 2013). Notably, Chen et al. (2016) included core and beam protons, α-particles, and electrons in their multi-fluid analysis of temperature anisotropy instabilities.

Despite this large body of work on the interplanetary solar wind, few recent efforts have been made to explore instability limits on proton temperature anisotropy in the magnetosheath. The 1990s did see a series of studies in this vein, but most relied on relatively small data sets and largely focused only on the case of $T_{\perp {\rm p}} > T_{\parallel {\rm p}}$. Anderson et al. (1994) found evidence of both ion–cyclotron and mirror modes in the magnetosheath but in distinct regions therein. A subsequent study (Anderson et al. 1996) identified and explored a series of periods of enhanced electromagnetic ion–cyclotron activity and found indications of instability-driven limits on $R_{\rm p}$. Gary et al. (1995) and Tan et al. (1998) likewise found strong indications that the ion–cyclotron instability acts in the magnetosheath. Phan et al. (1994, 1996) focused on the mirror instability and revealed that it too plays a role in regulating the temperature anisotropy of magnetosheath protons.

The present study is the first to use *MMS* observations of the magnetosheath to search for $\beta_{\parallel {\rm p}}$-dependent limits on $R_{\rm p}$-values (both $R_{\rm p} < 1$ and $R_{\rm p} > 1$) and to explore what role kinetic microinstabilities play in generating them. Although unstable modes, especially mirror and ion–cyclotron modes, have long been observed in the magnetosheath (e.g., Lucek et al. 2005; Soucek & Escoubet 2011; Wang et al. 2017, and references therein), the analysis herein focuses on understanding how instabilities affect proton temperature anisotropy.

3. Observations

MMS (Burch et al. 2016) consists of a constellation of four, virtually identical spacecraft that carry instruments optimized for measuring the plasma in and around Earth's magnetosphere (including the magnetosheath) with unprecedented resolution. All *MMS* data products are publicly available via the mission's Science Data Center (SDC): https://lasp.colorado.edu/mms/sdc/.

For this study, proton data were taken from the Dual Ion Spectrometer (DIS), which is a part of the Fast Plasma Investigation (FPI) (Pollock et al. 2016). In burst mode, FPI/DIS returns one distribution of ion energies every 150 ms. Each distribution provides values for one set of proton moments (including $n_{\rm p}$, $T_{\perp {\rm p}}$, and $T_{\parallel {\rm p}}$), which are hosted on the SDC.

The magnetic field data were derived from the Flux Gate Magnetometers (FGM) (Russell et al. 2016) in the FIELDS instrument suite (Torbert et al. 2016). In burst mode, FIELDS/FGM provides measurements of the $\boldsymbol{B}$ at a cadence of 128 Hz.

4. Analysis

This study utilized a data set consisting of *MMS* burst-mode measurements from six distinct periods, which are listed in

[9] Such a plot is sometimes informally referred to as a "Brazil plot" after the shape of the distribution often seen in the solar wind; see, e.g., Figures 1 and 2 in this work and Figure 1 by Hellinger et al. (2006).

Table 1
Periods of *MMS* Burst-mode Data Used in This Study

Date	Time Period		Median Conditions				
			n_p (cm^{-3})	$T_{\|p}$ (eV)	R_p	B (nT)	$\beta_{\|p}$
2016 Jan 11	00:57:04	01:00:34	52.	206.	1.09	27.1	6.3
2016 Jan 24	23:36:14	23:47:34	33.	342.	0.99	18.8	12.6
2016 Oct 25	09:45:54	09:54:34	187.	282.	1.02	43.5	11.3
2017 Jan 18	00:45:53	00:49:43	198.	115.	0.97	26.9	12.9
2017 Jan 27	08:02:03	08:08:03	15.	655.	1.01	20.1	9.6
2017 Nov 23	03:57:43	04:01:03	22.	241.	1.05	15.6	7.9

Table 1. These periods were originally studied by Chasapis et al. (2017, 2018) and were chosen because they provide relatively long intervals of magnetosheath measurements and showed strong indications of turbulence activity. Two of these periods had particularly high densities ($n_p > 100\,\mathrm{cm}^3$), but the ion count rates remained $\lesssim$4 MHz and were localized in the energy scans. Thus, significant saturation of the instrument is unlikely to have occurred (McFadden et al. 2008; Pollock et al. 2016), and the DIS estimates of temperature and density are deemed to be of sufficient quality for this study.

No multi-spacecraft techniques were employed in this study: each of the four *MMS* spacecraft was treated as an independent observer. Each spacecraft's ion and magnetic field measurements were synchronized, and the latter were averaged down to match the 150 ms cadence of the former. This ultimately produced a data set consisting of $N = 58{,}510$ measurements of the proton moments and the magnetic field.

Figure 1 shows the distribution of ($\beta_{\|p}$, R_p)-values in this data set. To generate this plot, the ($\beta_{\|p}$, R_p)-plane was divided into a grid of bins: 30 $\beta_{\|p}$-bins (logarithmically spaced from 1 to 10^3) by 30 R_p-bins (linearly spaced from 0.7 to 1.6). The color of each bin indicates, on a logarithmic scale, n, the number of data from the data set that it contains.

Since the binning of data in Figure 1 was arbitrary, Figure 2 was generated to show a more fundamental quantity than "counts per bin." Note that the two plots in Figure 2 are identical except for the overlaid curves, which are addressed below. The plots themselves were generated by binning the data set according to the same method used for Figure 1. Bins with $n < 10$ data were deemed statistically insignificant and suppressed. Following the method of Maruca et al. (2011), the plots show, for the statistically significant bins,

$$\tilde{p}(\beta_{\|p}, R_p) = \frac{n}{N\,\Delta\beta_{\|p}\,\Delta R_p}, \tag{3}$$

where n is the number of data in the bin, N is the total amount of data in the data set, and $\Delta\beta_{\|p}$ and ΔR_p are the widths of the bin along each axis. Thus, each value $\tilde{p}(\beta_{\|p}, R_p)$ estimates the value of $p(\beta_{\|p}, R_p)$, the probability density of observing a given set of ($\beta_{\|p}$, R_p)-values.

The overlaid curves in Figure 2 show contours of constant instability growth-rate, γ, across the ($\beta_{\|p}$, R_p)-plane. As is typical, $\gamma(\beta_{\|p}, R_p)$ is taken to be the growth rate of the fastest-growing mode for that set of ($\beta_{\|p}$, R_p)-values and is normalized

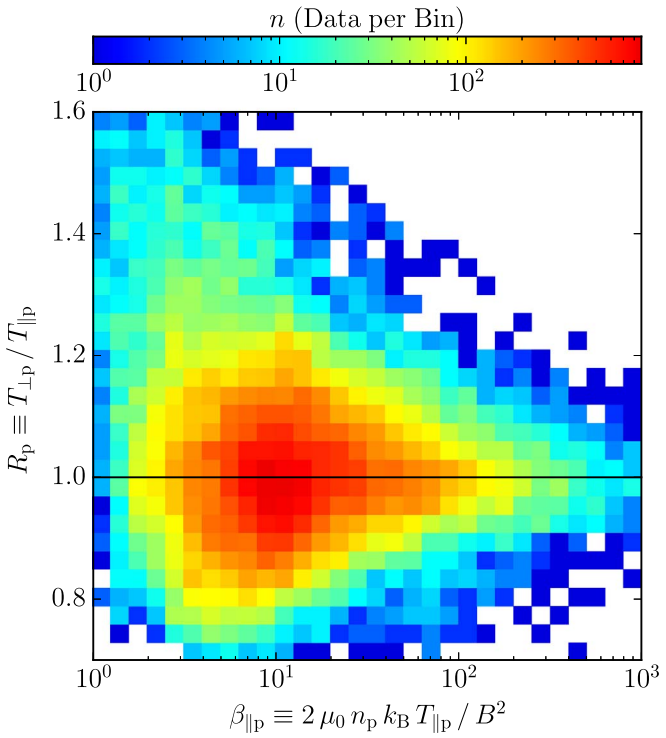

Figure 1. Plot of the distribution of ($\beta_{\|p}$, R_p)-values in the *MMS* data set specified in Table 1.

to the proton cyclotron frequency,

$$\Omega_p = \frac{q_p\,B}{m_p}, \tag{4}$$

where q_p and m_p are, respectively, the charge and mass of a proton. The contours on the left plot correspond to the parallel instabilities: the ion–cyclotron ($R_p > 1$) and parallel-firehose ($R_p < 1$). Those on the right plot correspond to the oblique instabilities: the mirror ($R_p > 1$) and oblique-firehose ($R_p < 1$). All of these contours were calculated using the same linear Vlasov software described by Maruca et al. (2012), which considers a plasma where each population of particles has a bi-Maxwellian VDF. For the present study, electrons were assumed to be isotropic. Likewise, the presence of proton beams and α-particles was neglected (due to the unavailablity of data on these populations in the *MMS*/FPI/DIS moments data set).

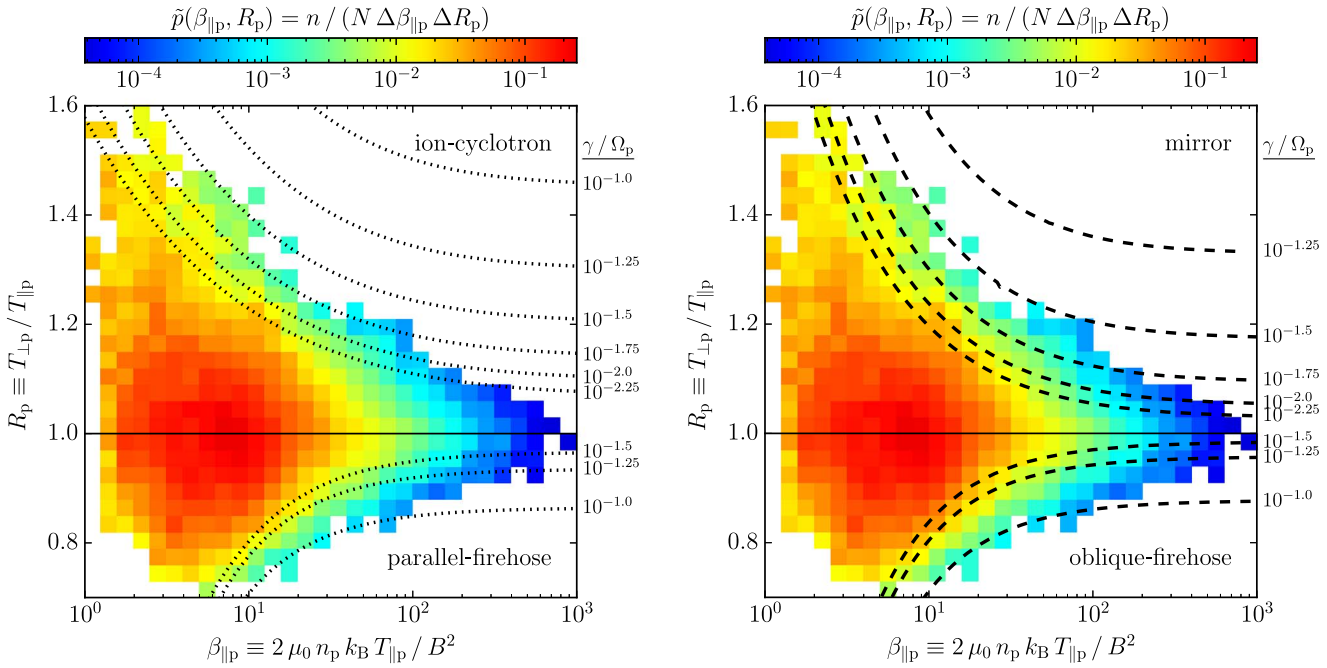

Figure 2. Two plots of the estimated probability density, $\tilde{p}$, of $(\beta_{\parallel p}, R_p)$-values (see Equation (3)) for the *MMS* data set specified in Table 1. These plots are identical except for the overlaid curves, which show contours of constant growth rate for different instabilities. The dotted curves (left) show the parallel instabilities: the ion–cyclotron ($R_p > 1$) and parallel-firehose ($R_p < 1$). The dashed curves (right) show the oblique instabilities: the mirror ($R_p > 1$) and oblique-firehose ($R_p < 1$). Each contour is labeled with its growth rate, γ, in units of the proton cyclotron frequency, Ω_p (see Equation (4)).

5. Discussion

Figures 1 and 2 strongly indicate the activity of $\beta_{\parallel p}$-dependent constraints on proton temperature anisotropy, R_p, in the Earth's magnetosheath. For any given $\beta_{\parallel p}$-value, a distribution of R_p-values is observed with a mode near $R_p \approx 1$. Nevertheless, the width of these R_p-distributions narrows considerably with increasing $\beta_{\parallel p}$. Thus, the magnetosheath likely hosts processes that favor isotropic proton temperatures (limiting both $R_p > 1$ and $R_p < 1$) and become more active at higher values of $\beta_{\parallel p}$.

These $\beta_{\parallel p}$-dependent constraints on R_p most likely arise from local processes in the magnetosheath. Similar constraints have long been observed in the interplanetary solar wind (e.g., Gary et al. 2001; Kasper et al. 2002; Hellinger et al. 2006), but this plasma undergoes significant increases in density and temperature as it crosses Earth's bow shock. For example, Maruca et al. (2011) found the mode of $\beta_{\parallel p}$ in near-Earth interplanetary solar wind to be ≈0.7, but for the magnetosheath plasma used in this study, the mode of $\beta_{\parallel p}$ is ≈8. Thus, the distribution of data in Figures 1 and 2 is unlikely to simply be a consequence of the similar distributions seen for the interplanetary solar wind.

Figure 2 suggests that microinstabilities play a role in limiting proton temperature anisotropy (both $R_p > 1$ and $R_p < 1$) in the magnetosheath. The plots in this figure show that the vast majority of $(\beta_{\parallel p}, R_p)$-values from this study's *MMS* data set fall within the limits of marginal stability set by linear Vlasov theory. Indeed, the observed contours of probability density over the $(\beta_{\parallel p}, R_p)$-plane align well with the predicted contours of constant instability growth rate. This behavior is consistent with instabilities limiting departures of proton temperature from isotropy (see, e.g., Matteini et al. 2012; Klein & Howes 2015).

The growth-rate contours computed for this study (and shown in Figure 2) are very similar for parallel and oblique instabilities (left and right plots, respectively). In contrast, for the lower-$\beta_{\parallel p}$ conditions of the interplanetary solar wind, these instabilities show much larger differences: especially for the ion–cyclotron and mirror thresholds ($R_p > 1$). Some studies (e.g., Hellinger et al. 2006; Bale et al. 2009; Maruca et al. 2011) counterintuitively found that the distribution of $(\beta_{\parallel p}, R_p)$-values observed in interplanetary solar wind more closely align with the mirror threshold even though the ion–cyclotron threshold typically sets a stronger constraint. No definitive assessment of the relative activity of the mirror and ion–cyclotron in the magnetosheath is possible in this study because the corresponding thresholds are so similar at high $\beta_{\parallel p}$. Qualitatively, Figure 2 seems to show that the mirror instability contours (with their sharper fall-off) align slightly better with the contours of $\tilde{p}(\beta_{\parallel p}, R_p)$ than those of the ion–cyclotron instability. Nevertheless, the difference is so minor that no clear conclusion can be drawn.

The results of this preliminary study motivate further investigation to understand how temperature anisotropy constraints arise in the magnetosheath and how they impact the large-scale evolution of the plasma. The standard view, reflected in much of our discussion above, is that the occurrence of linear instability near the periphery of the $(\beta_{\parallel p}, R_p)$-distribution signifies the role of these instabilities in establishing the limits of the distribution. The present results are consistent with this view and extend the surrounding questions to the magnetosheath. Future work might profitably employ a substantially larger data set of *MMS* observations to enable more definite conclusions about which instabilities (e.g., the mirror versus the ion–cyclotron) principally constrain R_p-values. It would be especially important to explore how the $(\beta_{\parallel p}, R_p)$-distribution varies across the different regions of the magnetosheath and with changes in plasma conditions. The

periods used in this study were chosen based on the availability of burst-mode measurements which, by definition, are only available from the small fraction of the spacecraft's trajectory. Thus, from this study alone, it is difficult to assess how ubiquitous instability-driven constraints on proton temperature anisotropy are in the magnetosheath.

This study should also be extended to incorporate measurements from other *MMS* instruments. Measurements of other ion species and of electrons should be explored for evidence of β-dependent constraints on their temperature anisotropies. Indications of such constraints have already been identified in the magnetosheath for electrons (Gary et al. 2005) and in the interplanetary solar wind for α-particles (Maruca et al. 2012; Bourouaine et al. 2013; Chen et al. 2016) and electrons (Štverák et al. 2008; Chen et al. 2016). Efforts should also be made to understand how the occurrence of temperature anisotropy constraints correlate with turbulent structures and fluctuations. Such correlations have been observed in the interplanetary solar wind (Osman et al. 2012, 2013) and identified in turbulence simulations of plasma at intermediate $\beta_{\|\mathrm{p}}$ (Servidio et al. 2014) and at high $\beta_{\|\mathrm{p}}$ (Kunz et al. 2014, 2016). The statistical association of temperature anisotropy constraints with enhancements in turbulence-generated coherent structures (e.g., current sheets) raises the possibility that such structures are involved in generating temperature anisotropy. Conversely, kinetic microinstabilities may provide a mechanism by which temperature anisotropy can generate turbulence. The theoretical investigation of Schekochihin et al. (2008) presented an example of how the nonlinear phase of an unstable mode can produce magnetic structures. This possibility is consistent with the observations of Bale et al. (2009), who found enhancements in magnetic fluctuations in marginally unstable plasma.

Effort on this study at the University of Delaware was partially supported by NASA HSR Grant NNX17AI25G, NASA LWS Grant NNX17AB79G, and *MMS* through NASA Grant NNX14AC39G. T.N.P. was supported by NSF Grant 1460130. W.H.M. is a member of the *MMS* Theory and Modeling Team.

This study used Level 2 FPI and FIELDS data products in cooperation with the instrument teams and in accordance with their guidelines. These and all *MMS* data are available at https://lasp.colorado.edu/mms/sdc/. We thank the SDC, FPI, and FIELDS teams for their assistance with this study.

B.A.M. thanks N. Godbole for feedback on this manuscript. The preparation of this manuscript made use of the SAO/NASA Astrophysics Data System (ADS): http://adsabs.harvard.edu/.

ORCID iDs

Bennett A. Maruca https://orcid.org/0000-0002-2229-5618
A. Chasapis https://orcid.org/0000-0001-8478-5797
S. P. Gary https://orcid.org/0000-0002-4655-2316
R. Bandyopadhyay https://orcid.org/0000-0002-6962-0959
R. Chhiber https://orcid.org/0000-0002-7174-6948
T. N. Parashar https://orcid.org/0000-0003-0602-8381
W. H. Matthaeus https://orcid.org/0000-0001-7224-6024
M. A. Shay https://orcid.org/0000-0003-1861-4767
C. J. Pollock https://orcid.org/0000-0001-9228-6605
D. J. Gershman https://orcid.org/0000-0003-1304-4769

References

Anderson, B. J., Denton, R. E., Ho, G., et al. 1996, JGRA, 101, 21527
Anderson, B. J., Fuselier, S. A., Gary, S. P., & Denton, R. E. 1994, JGRA, 99, 5877
Bale, S. D., Kasper, J. C., Howes, G. G., et al. 2009, PhRvL, 103, 211101
Bourouaine, S., Verscharen, D., Chandran, B. D. G., Maruca, B. A., & Kasper, J. C. 2013, ApJL, 777, L3
Burch, J. L., Moore, T. E., Torbert, R. B., & Giles, B. L. 2016, SSRv, 199, 5
Chasapis, A., Matthaeus, W. H., Parashar, T. N., et al. 2017, ApJ, 836, 247
Chasapis, A., Matthaeus, W. H., Parashar, T. N., et al. 2018, ApJL, 856, L19
Chen, C. H. K., Matteini, L., Schekochihin, A. A., et al. 2016, ApJL, 825, L26
Gary, S. P. 1993, Theory of Space Plasma Microinstabilities (Cambridge: Cambridge Univ. Press)
Gary, S. P., Lavraud, B., & Thomsen, M. F. 2005, GeoRL, 32, L13109
Gary, S. P., Skoug, R. M., Steinberg, J. T., & Smith, C. W. 2001, GeoRL, 28, 2759
Gary, S. P., Thomsen, M. F., Yin, L., & Winske, D. 1995, JGRA, 100, 21961
Gary, S. P., Wang, J., Winske, D., & Fuselier, S. A. 1997, JGR, 102, 27159
Hellinger, P., & Trávníček, P. 2014, ApJL, 784, L15
Hellinger, P., Trávníček, P., Kasper, J. C., & Lazarus, A. J. 2006, GeoRL, 33, 9101
Kasper, J. C., Lazarus, A. J., & Gary, S. P. 2002, GeoRL, 29, 20
Klein, K. G., Alterman, B. L., Stevens, M. L., Vech, D., & Kasper, J. C. 2018, PhRvL, 120, 205102
Klein, K. G., & Howes, G. G. 2015, PhPl, 22, 032903
Kunz, M. W., Schekochihin, A. A., & Stone, J. M. 2014, PhRvL, 112, 205003
Kunz, M. W., Stone, J. M., & Quataert, E. 2016, PhRvL, 117, 235101
Lucek, E. A., Constantinescu, D., Goldstein, M. L., et al. 2005, SSRv, 118, 95
Maruca, B. A., Kasper, J. C., & Bale, S. D. 2011, PhRvL, 107, 201101
Maruca, B. A., Kasper, J. C., & Gary, S. P. 2012, ApJ, 748, 137
Matteini, L., Hellinger, P., Landi, S., Trávníček, P. M., & Velli, M. 2012, SSRv, 172, 373
Matteini, L., Landi, S., Hellinger, P., et al. 2007, GeoRL, 34, 20105
McFadden, J. P., Carlson, C. W., Larson, D., et al. 2008, SSRv, 141, 477
Osman, K. T., Matthaeus, W. H., Hnat, B., & Chapman, S. C. 2012, PhRvL, 108, 261103
Osman, K. T., Matthaeus, W. H., Kiyani, K. H., Hnat, B., & Chapman, S. C. 2013, PhRvL, 111, 201101
Phan, T. D., Larson, D. E., Lin, R. P., et al. 1996, GeoRL, 23, 1279
Phan, T.-D., Paschmann, G., Baumjohann, W., Sckopke, N., & Lühr, H. 1994, JGRA, 99, 121
Pollock, C., Moore, T., Jacques, A., et al. 2016, SSRv, 199, 331
Russell, C. T., Anderson, B. J., Baumjohann, W., et al. 2016, SSRv, 199, 189
Schekochihin, A. A., Cowley, S. C., Kulsrud, R. M., Rosin, M. S., & Heinemann, T. 2008, PhRvL, 100, 081301
Schwartz, S. J. 1980, RvGSP, 18, 313
Servidio, S., Osman, K. T., Valentini, F., et al. 2014, ApJL, 781, L27
Soucek, J., & Escoubet, C. P. 2011, AnGeo, 29, 1049
Štverák, S., Trávníček, P., Maksimovic, M., et al. 2008, JGRA, 113, A03103
Tan, L. C., Fung, S. F., Kessel, R. L., et al. 1998, GeoRL, 25, 587
Torbert, R. B., Russell, C. T., Magnes, W., et al. 2016, SSRv, 199, 105
Treumann, R. A., & Baumjohann, W. 1997, Advanced Space Plasma Physics (London: Imperial College Press)
Verscharen, D., Chandran, B. D. G., Klein, K. G., & Quataert, E. 2016, ApJ, 831, 128
Wang, X. Y., Huang, S. Y., Allen, R. C., et al. 2017, JGRA, 122, 8228
Wicks, R. T., Matteini, L., Horbury, T. S., Hellinger, P., & Roberts, D. A. 2013, in AIP Conf. Ser. 1539, Solar Wind 13, ed. G. P. Zank et al. (Melville, NY: AIP), 303
Yoon, P. H. 2017, RvMPP, 1, 4